Structural Characterization of the Caveolin Scaffolding Domain in Association with Cholesterol-Rich Membranes

Cody L. Hoop,[†] V. N. Sivanandam,[†,‡] Ravindra Kodali, Matthew N. Srnec, and Patrick C. A. van der Wel*

Department of Structural Biology, University of Pittsburgh School of Medicine, Biomedical Science Tower 3, 3501 Fifth Ave., Pittsburgh, Pennsylvania 15260, United States

ⓢ *Supporting Information*

ABSTRACT: Members of the caveolin protein family are implicated in the formation of caveolae and play important roles in a number of signaling pathways and in the regulation of various proteins. We employ complementary spectroscopic methods to study the structure of the caveolin scaffolding domain (CSD) in caveolin-1 fragments, while bound to cholesterol-rich membranes. This key domain is thought to be involved in multiple critical functions that include protein recognition, oligomerization, and cholesterol binding. In our membrane-bound peptides, residues within the flanking intramembrane domain (IMD) are found to adopt an α-helical structure, consistent with its commonly believed helical hairpin conformation. Intriguingly, in these same peptides, we observe a β-stranded conformation for residues in the CSD, contrasting with earlier reports, which commonly do not reflect β-structure. Our experimental data based on solid-state NMR, CD, and FTIR are found to be consistent with computational analyses of the secondary structure preference of the primary sequence. We discuss how our structural data of membrane binding Cav fragments may match certain general features of cholesterol-binding domains and could be consistent with the role for CSD in protein recognition and homo-oligomerization.
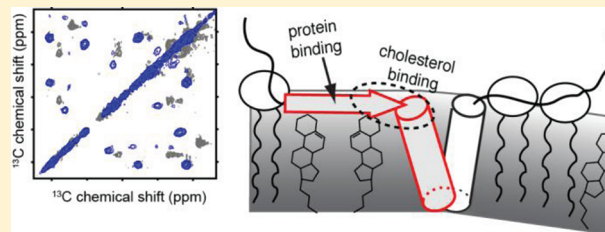
Caveolae are flask-shaped and cholesterol-rich invaginations in plasma membranes found to participate in many cellular functions across various cell types.[1−3] Their roles include lipid uptake and regulation, molecular transport, cell adhesion, and signal transduction.[2,3] The caveolin family of proteins is thought to play a central role in the formation and functioning of these lipid-raft-like domains. There are three isoforms, caveolin-1 (Cav1), caveolin-2, and caveolin-3, of which Cav1 is the most common. Found in a wide array of mammalian cells, Cav1 is implicated in multiple diseases, including cancers and muscular disease.[4,5] It contains cytoplasmic N- and C-terminal domains that sandwich the membrane-association domains: the caveolin scaffolding domain (CSD; residues 82−101) and the intramembrane domain (IMD) spanning roughly residues 102−134 (Figure 1).[1] The latter is thought to form a unique α-helical hairpin that does not completely traverse the membrane.[4,6,7] These domains are assisted in their membrane-binding roles by three palmitoylated cysteines, which are not essential for localization to caveolae,[8−10] but do appear critical for other functionality, such as the transportation of cholesterol.[10]

The most prominent domain is the CSD, as residues within it not only are responsible for membrane binding but also are critical for oligomerization, protein interactions, and cholesterol recognition.[11,12] Residues within the CSD are required for oligomerization of Cav monomers into homo-oligomers of 14−16 proteins, which themselves assemble into higher-order oligomers during the formation of caveolae.[11] On top of this, the $F_{92}TVT_{95}$ segment within the CSD is important for signaling, as it is required for interaction with binding protein
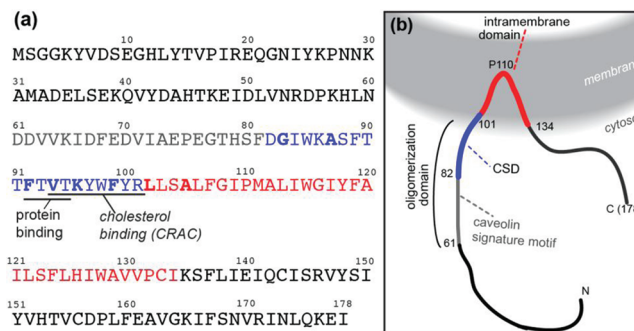

Figure 1. Primary sequence and schematic illustration of caveolin-1. Key domains are indicated: the CSD in blue, containing the cholesterol-binding CRAC motif and the residues required for binding of protein partners (underlined). Bold residues indicate sites U−[13]C,[15]N-labeled in one or more peptides.

partners (e.g., G-protein α-subunits).[11,13,14] This binding event involves a consensus motif in the partner protein with high aromatic content, sometimes referred to as a caveolin-binding motif (CBM). A similar motif is also found in caveolin itself, raising the possibility of structural similarities between protein partner binding and Cav homo-oligomerization.[14] Finally, the CSD is ascribed a role in the recognition and binding of

cholesterol, which is highly concentrated in caveolae and needed for their formation. More precisely, formation of caveolae strictly requires tight binding of Cav to cholesterol.[15] This functionality is thought to localize to a cholesterol recognition/interaction amino acid consensus (CRAC) motif[2] in residues V_{94}TKYWFYR$_{101}$.[16] Thus, despite its short length, this 20-residue segment appears to incorporate an array of critical functionalities in overlapping sequence elements.

Unfortunately, its molecular mechanism of action and structural features remain unclear. Many reports indicate significant but varying degrees of α-helical structure in the CSD. A number of experimental studies have reported partially or even extensively α-helical CSD.[16,17] This is in part supported by computational analysis of the primary sequence.[4,17−20] A helical conformation has been employed to rationalize Cav1 binding partner recognition via the CSD[21] as well as the cholesterol-binding of CRAC motifs in general.[22] Comparisons of the various experimental studies are complicated by differing sample conditions and Cav1 constructs, some of which are rather short fragments.[16,20] It has been suggested that use of overly short Cav1 fragments may have caused a loss of helicity due to peptides being truncated within secondary structure elements.[17] Experimental conditions also often involve vesicular or micellar samples that lack cholesterol and may not emulate the native, highly cholesterol-rich membrane environment of the caveolae.[23] In contrast to most other studies, an integrative bioinformatics study by Spisni et al. suggested an antiparallel β-hairpin for residues 84−94, based on their computational analysis and previous functional and mutational results.[24]

To explore some of these ambiguities regarding the structure of Cav1, particularly the CSD, we here present results from our studies of Cav1 fragments in cholesterol-rich lipid bilayer samples. Through the use of solid-state NMR (ssNMR), we examine the structure of the peptide fragments while bound to the membrane and also observe their modulation of the membrane structure and dynamics. Solid-state NMR is a powerful tool for membrane protein studies, as it is compatible with a wide range of sample compositions and allows characterization of both lipids and proteins or peptides.[25−27] This applies to both magic-angle-spinning (MAS) NMR measurements and "static" experiments on pelleted or aligned membranes. Indeed, previous work on shorter CSD fragments employed ssNMR for the characterization of their effect on the membrane.[16] We perform static and MAS ssNMR experiments, supported with circular dichroism (CD) and Fourier transform infrared (FTIR) spectroscopy to probe selected Cav1 fragments. These include a short peptide that reflects the isolated CSD (Cav$_{83−102}$) and a longer construct (Cav$_{82−109}$), which incorporates part of the IMD. Previous reports suggested that the former has a mixed secondary structure but that the latter has a predominantly α-helical conformation, at least in dodecylphosphocholine (DPC) micelles.[16,17] Here, we examine their structures in cholesterol-rich lipid bilayers designed to more closely mimic caveolae, which should provide a better context to probe the cholesterol-binding and oligomerization characteristics of these peptides. Our CD and FTIR data indicate an increased α-helicity in the longer peptide (in agreement with some earlier reports), but ssNMR reveals that this α-helicity is specifically located in the putative first helix of the IMD and that residues within the CSD segment adopt a β-sheet conformation even in the presence of the flanking IMD. This turns out to be consistent with structural propensities of these fragments, as well as full-length Cav1, as indicated by various primary-sequence-based secondary structure prediction algorithms. We conclude by discussing our observations in the light of previous reports, along with possible implications for the structure and function of caveolin and its multifaceted scaffolding domain.

■ EXPERIMENTAL PROCEDURES

Sample Preparation. Appropriately Fmoc- and side-chain-protected ^{13}C, ^{15}N-labeled amino acids were purchased from Cambridge Isotope Laboratories (Andover, MA) and Isotec (Sigma-Aldrich, St. Louis, MO). Site-specifically ^{13}C, ^{15}N-labeled and unlabeled peptides (Table S1) were synthesized by Fmoc solid-phase chemistry and purified via reversed phase HPLC to greater than 95% purity by the W.M. Keck Facility at Yale University and New England Peptides (Gardner, MA). 1-Palmitoyl-2-oleoyl-*sn*-glycero-3-phosphocholine (POPC) was obtained from Avanti Polar Lipids (Alabaster, AL), and cholesterol was obtained from Sigma-Aldrich (St. Louis, MO); both were used without further purification. Membrane samples containing a 1:1 molar ratio of phospholipid/cholesterol were prepared following modifications of previously published protocols.[16,28] Peptide dissolved in trifluoroethanol (TFE) was combined with codissolved phospholipid and cholesterol in chloroform/methanol (2/1, v/v). A dry peptide/lipid/cholesterol film, obtained by drying under a N_2-stream and overnight exposure to high vacuum, was resuspended in excess HEPES buffer (20 mM HEPES with 1 mM EDTA and 150 mM NaCl at pH 7.0), sonicated for 10−15 min, and subjected to several cycles of freeze−thawing. Negatively stained transmission electron microscopy and dynamic light scattering measurements (not shown) indicated the resulting vesicles were typically ∼100 nm in diameter.

Solid-State NMR. Membrane samples, with or without peptide (typically 10 mol %), were pelleted into 4 mm or 3.2 mm zirconia MAS rotors (Bruker Biospin, Billerica, MA) by centrifugation and were kept fully hydrated and unfrozen at all times. All experiments were carried out on a wide-bore Bruker Avance I spectrometer operating at 600 MHz ^{1}H Larmor frequency (14.3T) using either a Bruker wide-bore 4 mm CPMAS triple channel or standard-bore 3.2 mm CPMAS EFree HCN probe. The MAS experiments employed a spinning rate $\omega_r/2\pi = 8$ kHz, while cooling the sample using precooled gas, at all times maintaining the sample temperature above the phase transition temperature of the lipids. Static and MAS ^{31}P spectra were acquired with a wide-bore 4 mm double-channel (^{1}H,^{31}P) CP MAS probe (Bruker) in the absence and presence of sample spinning, applying 50 kHz two-pulse phase modulation (TPPM) ^{1}H decoupling.[29] Line shape analysis and integration were performed using Topspin software (Bruker Biospin, Billerica, MA). ^{31}P chemical shifts were referenced to phosphoric acid via external referencing to hydroxyapatite.[30] Assignments of peptide resonances were primarily carried out through analysis of 2D ^{13}C−^{13}C experiments employing ^{1}H−^{13}C cross-polarization (CP) followed by 25−100 ms DARR mixing[31] with 83 kHz TPPM decoupling during acquisition and evolution. Long distance contacts were observed via 2D ^{13}C−^{13}C experiments utilizing 400 ms PDSD mixing with 71−83 kHz TPPM decoupling during acquisition and evolution. Assignments of the POPC and cholesterol resonances were done with reference to previously published literature and are supported by 2D ^{1}H−^{13}C HETCOR experiments (not shown).[32,33] Spectra
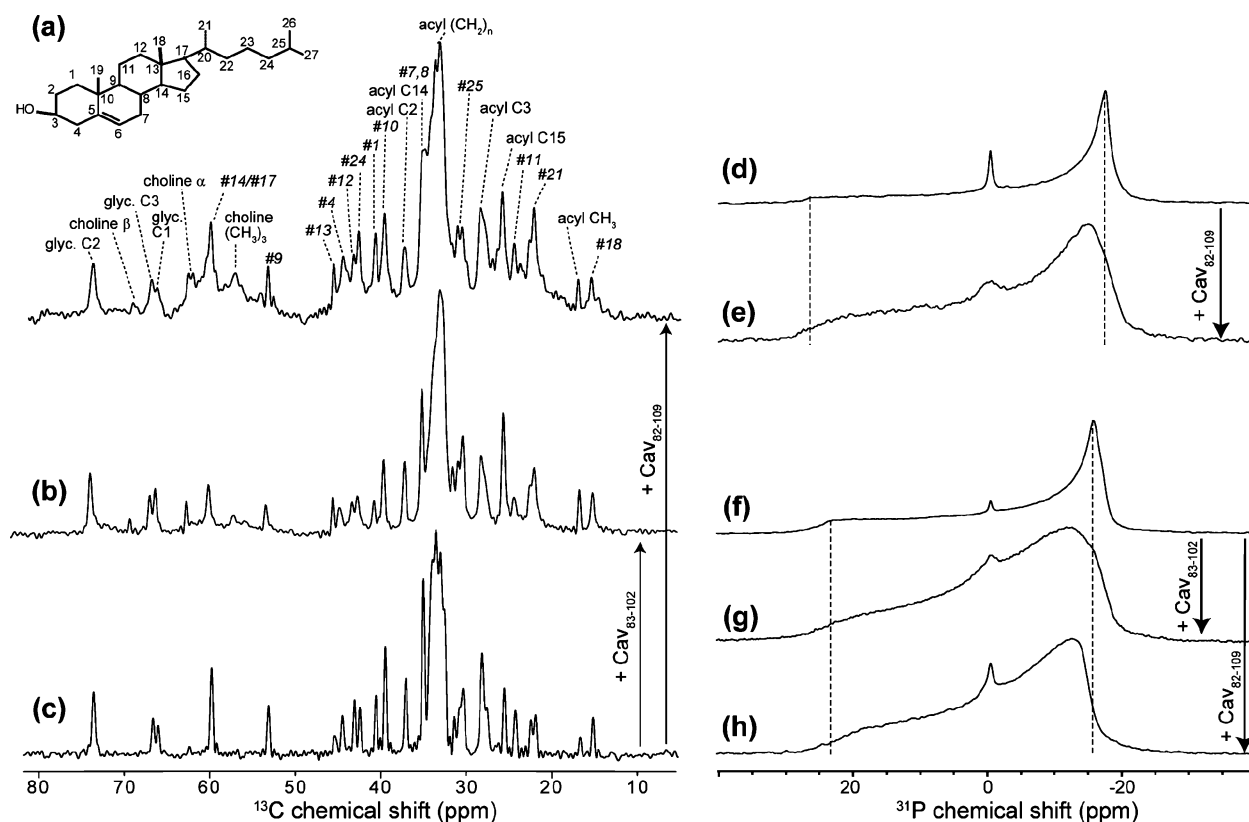
Figure 2. SSNMR shows effects of peptides on the membranes. $^1H-^{13}C$ CPMAS spectra of 1:1 POPC/cholesterol in presence of (a) 10 mol % Cav$_{82-109}$ (unlabeled), (b) 10 mol % Cav$_{83-102}$ (unlabeled), or (c) without peptide. Selected assignments of POPC and cholesterol are shown, the latter as italicized numbers (#; see inset). In presence of the peptides, ^{13}C signals throughout the lipids are broadened and some previously missing mobile POPC signals become visible. Static ^{31}P NMR of POPC without (d) or with (e) 10 mol % Cav$_{82-109}$, and 1:1 POPC/cholesterol in absence of peptide (f) or in presence of (g) 10 mol % Cav$_{83-102}$ or (h) 10 mol % Cav$_{82-109}$ shows that the lipids predominantly form a bilayer, with less than 5% present as isotropic signals. Peptide incorporation changes the lipid headgroup dynamics, seen as a reduction of the bilayer ^{31}P CSA (see dashed vertical lines). Measurements were done with full hydration, at 300 K and 600 MHz ^1H frequency.

were processed and analyzed using the Bruker Topspin,[34] NMRPipe,[34] Sparky,[35] and CCPNMR/Analysis programs.[36] ^{13}C chemical shifts were referenced to dilute aqueous DSS via external referencing to adamantane, and ^{15}N chemical shifts were indirectly referenced to liquid ammonia.[37] Additional experimental details are available in Table S2.

FTIR and CD Spectroscopy. For FTIR, samples containing 5 or 10 mol % Cav$_{82-109}$ or Cav$_{83-102}$ in 1:1 POPC/cholesterol or DPC micelles were obtained as pellets via centrifugation. The pellet was placed between two CaF$_2$ windows on an MB series spectrophotometer (ABB Bomem, Quebec City, QC, Canada) and analyzed with PROTA software (Biotools Inc., Jupiter, FL). Spectra were recorded at 4 cm^{-1} resolution and at room temperature (averaging over 400 scans). Buffer correction was applied by subtracting the buffer spectrum interactively until a flat baseline was obtained between 1700 and 1800 cm^{-1}. Peak volumes were estimated by fitting with Gaussian line shapes using the PeakFit routine in SigmaPlot (Systat Software, San Jose, CA).

Cav$_{82-109}$ and Cav$_{83-102}$ containing samples for CD were prepared in either POPC vesicles (1:100 peptide−lipid ratio) or DPC micelles (4 mM) in a 13.3 mM phosphate buffer at pH ~6.25, resulting in final peptide concentrations of 10−25 μM. CD spectra were recorded at 25 °C using a Jasco J-810 spectropolarimeter (Jasco Inc., Easton, MD), averaging over 10 scans with a scanning speed of 50 nm/min in steps of 1 nm.

Sequence Analysis and Secondary Structure Prediction. The secondary structure of full-length Cav1 and fragments Cav$_{82-109}$ and Cav$_{83-102}$ was predicted via selected algorithms. The PSIPRED (http://bioinf.cs.ucl.ac.uk/psipred), Proteus2 (http://wishart.biology.ualberta.ca/proteus2), and PredictProtein (http://www.predictprotein.org/) algorithms were accessed via their respective Web sites.[38−40]

■ RESULTS

Peptide Incorporation into Model Membranes Using Static and MAS ssNMR. In order to confirm the incorporation of the peptides into the lipid membranes and to probe their localization within the membrane, we applied a number of ssNMR experiments. In analogy with previous work,[16] we examined the peptides' effect on the lipids through basic ^{13}C and ^1H MAS NMR experiments. In our hands, the POPC and cholesterol chemical shift changes upon peptide introduction were relatively small and did not unequivocally identify more significant effects on particular parts of the lipids. In various independently prepared samples, introduction of CSD peptides does consistently cause a broadening of the carbon line widths, likely due to a decrease in membrane fluidity. Figure 2a−c shows the natural abundance ^{13}C signals from 1:1 POPC/cholesterol in presence of 10 mol % Cav$_{82-109}$ (a), with 10 mol % Cav$_{83-102}$ (b), or without peptide (c). It is notable that a single signal is observed for each lipid and
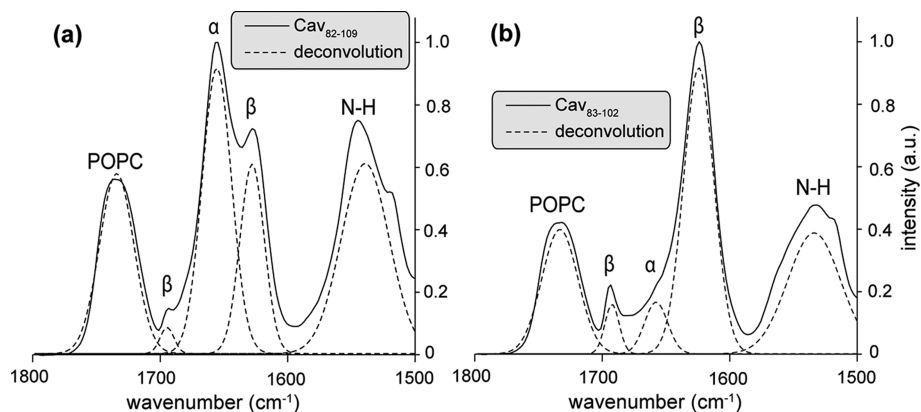
Figure 3. FTIR spectra of (a) 10 mol % Cav$_{82-109}$ and (b) 10 mol % Cav$_{83-102}$ in 1:1 POPC/cholesterol. Deconvolutions for estimating secondary structure content are shown as dashed for their respective data sets. Results are consistent with a mixed secondary structure in the longer peptide and predominantly β-sheet structure in the shorter construct.

cholesterol site, indicating a single homogeneously structured population of the lipids.

To probe the behavior of the phospholipid head groups, we applied static ^{31}P NMR experiments that are informative of the lipids' macroscopic assembly into distinct lipid phases and the dynamics of individual lipids. Static 1D ^{31}P NMR spectra of 1:1 POPC/cholesterol mixtures are dominated by broad signals with a line shape typical of uniaxial motional averaging of the ^{31}P chemical shift anisotropy (CSA) (Figure 2f) as part of the complex motions that characterize phospholipid bilayers.[41] The apparent uniaxial rotation reflects rapid Brownian motion of the phospholipids within the fluid bilayer. In addition to the bilayer phase, certain samples also feature a small isotropic peak (close to 0 ppm), constituting at most 5% of the overall intensity (as determined by line shape simulations). Such isotropic ^{31}P NMR signals indicate that a small portion of the phospholipid head groups undergoes rapid isotropic motional averaging, as is found in small vesicles, micelles, or highly curved nonbilayer phases.[42,43] Note that these isotropic signals are not specifically correlated to the presence of peptide but are also seen in lipid-only samples. Compared to POPC bilayers alone (panel d), introduction of high levels of cholesterol (panel f) leads to a notable decrease of the ^{31}P CSA.[44] This is most likely due to an increased wobbling motion of the PC headgroup,[41] which can be rationalized based on the fact that cholesterol mostly occupies the hydrophobic core of the membrane, lacks a large headgroup, and thus allows for more space and motion of the PC headgroup.[45]

In the presence of the Cav1 fragments, the PC head groups still show a dominant bilayer line shape (Figure 2g,h). The Cav1 peptides do significantly modulate the observed inhomogeneous and homogeneous line broadening of the lipid ^{31}P signals. They have a concentration-dependent (Figure S1) narrowing effect on the ^{31}P CSA. In analogy to cholesterol's effect, this may indicate incorporation into the membrane's hydrophobic core with less interaction with the lipid head groups. This decrease in the inhomogeneous broadening is more pronounced for the Cav$_{82-109}$ peptide (Figure 2h) than the isolated CSD (Figure 2g). Addition of the peptide also causes an *increase* in the homogeneous line width (Figure 2e,g,h). Such effects have previously been seen with other membrane-binding compounds and are most likely due to an interference with the overall motion of the phospholipids.[46] In POPC (Figure 2e) and, to a lesser extent, POPC/cholesterol

bilayers (Figure 2g,h), the rapid Brownian motion of each lipid in the fluid bilayer helps to reduce the $^{31}P-^{1}H$ dipolar interactions, which can otherwise cause an "intrinsic broadening" of the ^{31}P signal of individual lipids.[46,47] The incorporation of the Cav1 fragments interferes with the rapid lipid motion and thus results in an increased homogeneous broadening of the ^{31}P NMR line shape.

The above observations indicate an intimate interaction of these peptides with the lipid membranes, without signs of peptide-induced heterogeneity. The peptides seem to partition preferentially into the hydrophobic part of the bilayer, providing more space for POPC headgroup motion, while reducing the overall fluidity of the membrane.

Peptide Secondary Structure Content. Having probed the peptides' incorporation into the mixed membranes, we also characterized the secondary structure of the membrane-associated peptides. FTIR studies were performed on Cav$_{82-109}$ and Cav$_{83-102}$ peptides in a 1:1 POPC/cholesterol mixture, prepared identically to the NMR samples (Figure 3). Cav$_{82-109}$ features C=O vibrations characteristic for both α-helix (1654 cm^{-1}) and β-strand (1623 and 1693 cm^{-1}).[48] Based on peak deconvolution (see Figure 3), relative amounts of approximately 60% α-helical and 40% β-sheet are estimated for Cav$_{82-109}$ (Table S3). In contrast, the shorter Cav$_{83-102}$ displays little α-helical content (Figure 3b). The phospholipid's ester C=O vibration is also observed at 1730 cm^{-1}.[49]

The FTIR results thus indicate a notable increase in α-helical content in the longer peptide, an observation that is consistent with the work by Le Lan et al., employing CD spectroscopy.[17] These earlier studies were done in DPC rather than cholesterol/POPC membranes. We obtained similar FTIR results in DPC micelles (not shown) and CD spectra in POPC also indicated a low level of helicity in the shorter peptides and an increased α-helical content for the longer peptide (Figure S2).

Thus, both CD and FTIR indicate an increase in α-helical content in Cav$_{82-109}$, but it appears that a substantial fraction remains non-α-helical. These data do not indicate the localization of the helix and could be explained by sample heterogeneity.

Site-Specific Structure Analysis by MAS ssNMR. To site specifically probe the mixed secondary structure of Cav$_{82-109}$, MAS ssNMR was applied to partly $^{13}C,^{15}N$-labeled peptides. Two Cav$_{82-109}$ peptides with $^{13}C,^{15}N$-labeling of

residues in both the CSD and IMD were incorporated into 1:1 POPC/cholesterol membranes. The first peptide (p1) featured U$-^{13}$C,^{15}N-labeled residues in sites Ala87, Phe92, Val94, and Lys96, and the second (p2) was labeled in residues Gly83, Val94, Phe99, Leu102, and Ala105 (Table S1). Probing residues Phe92 and Val94 yields structural information on the FTVT protein binding segment,[13] while analogously measuring Val94, Lys96, and Phe99 provides insight into the CRAC motif.[16] Labeling of Val94 in both peptides permitted verification of unchanged Val94 shifts between different samples, which was indeed the case (Figure S3). Chemical shift assignments were obtained using 2D ^{13}C$-^{13}$C DARR[31] experiments (e.g., Figure 4), supplemented with 2D ^{15}N$-^{13}$C
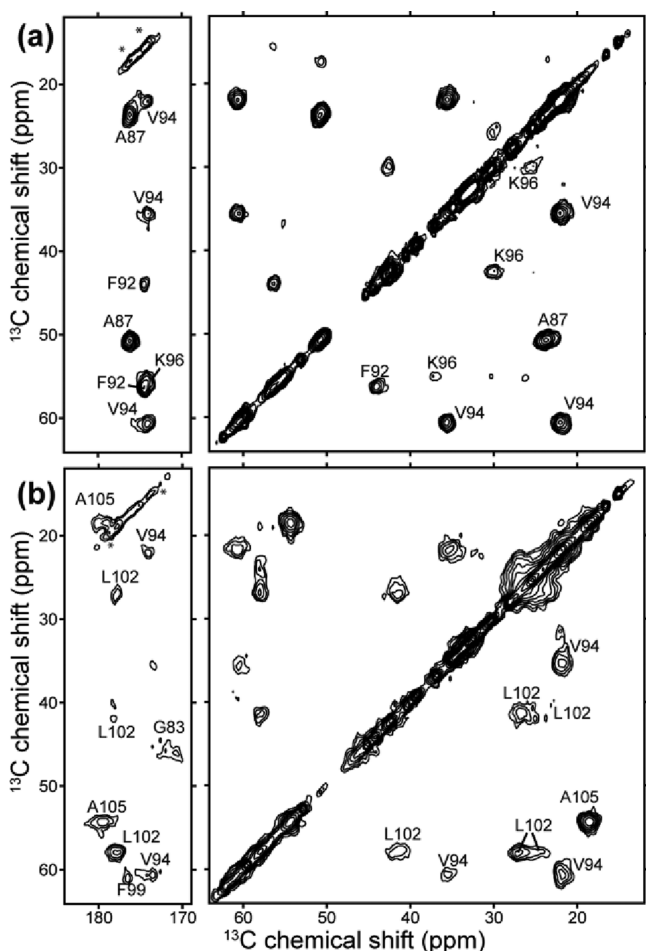

Figure 4. 2D ^{13}C$-^{13}$C ssNMR spectra using 25 ms DARR mixing, providing 1−2 bond transfers. Measurement on samples (a) p1 and (b) p2 are shown; both obtained at 600 MHz ^{1}H frequency and 8 kHz MAS at 283 K. Aliphatic-to-carbonyl (left) as well as intra-aliphatic (right) spectral regions are shown.

correlations (not shown), and are available in Table S4. In most cases single resonances were observed, indicating the presence of a single well-defined conformation, although motional averaging that is fast on the NMR time scale cannot be excluded. We do observe weaker additional resonances for Ala87 and Val94 (in both peptides), indicating a less-populated secondary conformation of those residues. Reduced intensities of certain peaks (e.g., the labeled Phe side chains) are consistent with conformational exchange of the amino acid side chains.

We examined the residue-specific secondary structure by comparing our chemical shifts to the corresponding shifts of known protein structures, in an approach known as chemical shift indexing (CSI).[50,51] The difference of ^{13}C chemical shifts from random coil shifts[51] correlates in a predictable fashion to the local secondary structure. As shown in Figure 5, these data indicate that residues Ala87, Phe92, Val94, and Lys96, spanning the protein binding and CRAC motifs, adopt a β-sheet conformation, whereas residues Phe99 (part of the CRAC motif), Leu102, and Ala105 (in the IMD) adopt an α-helical structure. Gly83, near the N-terminus of this peptide fragment, appears to lack a clearly defined secondary structure.

Given concerns about the effect of truncation of secondary structure elements,[17] we also examined a longer peptide Cav$_{76-109}$ (p3), which in the native sequence is flanked on both sides by prolines (P75 and P110), which often act as secondary structure breakers. Proline effects on membrane-spanning helices seems to be more subtle, yet they do tend to destabilize these α-helices.[52] We incorporated isotopic labels at Gly83 and Ala87 as probes of the CSD secondary structure and found that these residues had the same chemical shifts (and thus structures) as in the Cav$_{82-109}$ fragment (Figure S3).

The β-sheet and α-helical structural elements in Cav$_{82-109}$ were further probed in 2D ^{13}C$-^{13}$C experiments with 400 ms PDSD mixing. These conditions permit ^{13}C$-^{13}$C magnetization transfer over longer distances and revealed not only intra-residue contacts within labeled residues but also specific inter-residue contacts. As summarized in Figure 5, residue Val94 is observed to interact with both Phe92 and Lys96, consistent with $i \rightarrow i + 2$ contacts typical of β-sheet structure. Similarly, residue Leu102 interacts with residue Ala105, reflecting an $i \rightarrow i + 3$ contact characteristic of α-helical structure (and one that would not likely be observed in a β-strand). The observation of these $i \rightarrow i + 2$ and $i \rightarrow i + 3$ contacts are all consistent with the secondary structure elements identified from the CSI analysis above and further solidify the secondary structure assignments (Figure 5).

Structure Prediction. Our observations of a partially β-sheet structure localized within the CSD (specifically including the labeled residues between positions 87 and 96) seem to match results from a computational study that predicted an antiparallel β-hairpin motif in residues 84−94.[24] However, a number of other studies report a preference for α-helical structure from primary sequence analysis.[4,19] To explore this in more detail, we have also applied a number of prediction algorithms on full-length Cav1 and selected fragments. The results of predictions using the PSIPRED algorithm[38] are shown in Figure 6, suggesting a preference for an extended (possibly β-sheet) conformation throughout the CSD segment, followed by an α-helical structure in the IMD, not only in full length Cav1 but also in the Cav$_{82-109}$ fragment (gray box in Figure 6). Moreover, consistent with our and earlier experimental results,[17] truncation of the α-helical segment (i.e., ending at residue 102 rather than just before the native helix-breaker Pro110) is predicted to destabilize the helical conformation (e.g., in Cav$_{83-102}$). However, there appears to be little indication of a fully α-helical CSD. Similar results were obtained with the PROTEUS2 and PredictProtein prediction algorithms,[39,40] both of which suggest mixtures of β- and α-structure within the CSD (see Figure S4). Overall, the results of all three algorithms are also somewhat similar to the consensus results presented by Spisni et al, but differ from the reports of more extensive helical preferences. Of course, it remains unseen
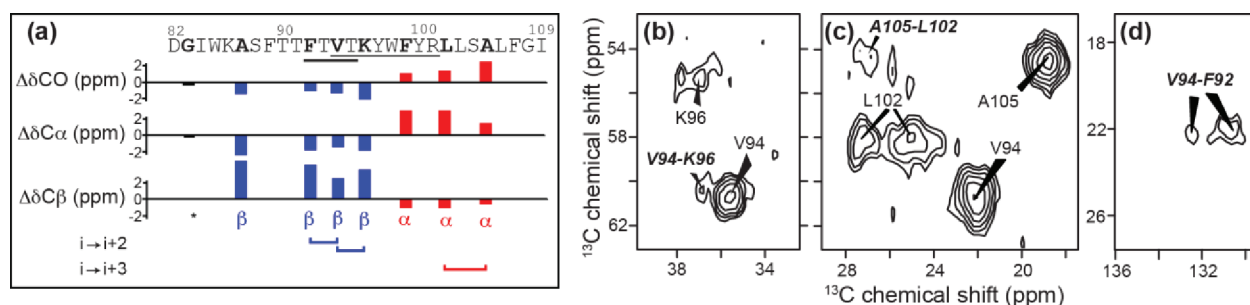
Figure 5. (a) SSNMR indicates α-helical conformation (red) for labeled sites in the IMD, while most CSD residues have a β-conformation (blue). Residues of the CRAC motif ($V_{94}-Y_{100}$) span the helix−strand boundary, and the protein binding motif ($F_{92}-T_{95}$) is in a β-strand. The CSI shows the difference ($\Delta\delta$) of C′, Cα, and Cβ chemical shifts from random coil values. Black bars lack a defined secondary structure (e.g., G83). Also indicated are the observations of $i \rightarrow i + 2$ contacts between F92−V94 and V94−K96 (b, d) and an $i \rightarrow i + 3$ contact between L102−A105 (c). The spectra are from long-distance $^{13}C-^{13}C$ experiments with 400 ms PDSD mixing, obtained at 600 MHz ^{1}H frequency and 8 kHz MAS at 283 K.
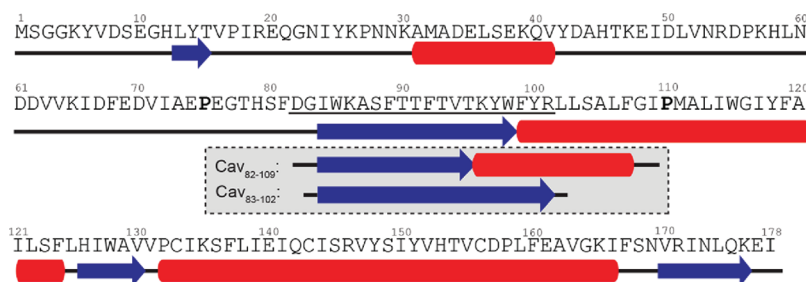

Figure 6. Secondary structure prediction of Cav1 and fragments. PSIPRED analysis of full-length Cav1 (Cav$_{1-178}$) indicates a propensity for β-sheet structure in the CSD (underlined). Predictions for fragments Cav$_{82-109}$ and Cav$_{83-102}$ (gray inset) suggest a sensitivity to helix truncation but always include a CSD with significant β-sheet structure.

how reliable any of these generally globular-protein-based algorithms will prove to be for this oligomerizing, cholesterol-binding and likely monotopic membrane protein.

◼ DISCUSSION

On the basis of a combination of ssNMR, CD, and FTIR measurements, we have characterized the secondary structure of Cav1 fragments, while bound to cholesterol-rich model membranes. These experiments were designed to examine the CSD, as it harbors many Cav1 functionalities. The Cav$_{82-109}$ peptide, incorporating both the CSD and the first half of the IMD, was found to contain a mixture of β-sheet and α-helical structure. The latter was localized within the putative first α-helix of the helical hairpin of the IMD, consistent with previous work and structural models and predictions.[17−20] More surprisingly, our observations indicate a β-strand conformation for the majority of labeled residues within the CSD, based on ssNMR shift analysis and inter-residue contacts, as well as the detection of mixed secondary structure by CD and FTIR. Computational analysis of the primary sequence predicts that part of the CSD prefers a β-sheet conformation and matches both the location of the experimental transition to α-helix and the observed lack of helicity in short peptides.[17,24] Figure 7 contains a graphical schematic that summarizes these observations. The observed helicity of the first half of the IMD is consistent with reports proposing models where the P110 forms the turn in a "re-entrant" helix stabilized by interacting smaller residues in both its helical segments.[4,6,7] This domain's wedge shape that fails to traverse the entire bilayer may well contribute to the remarkable membrane curvature of the caveolae.[53]
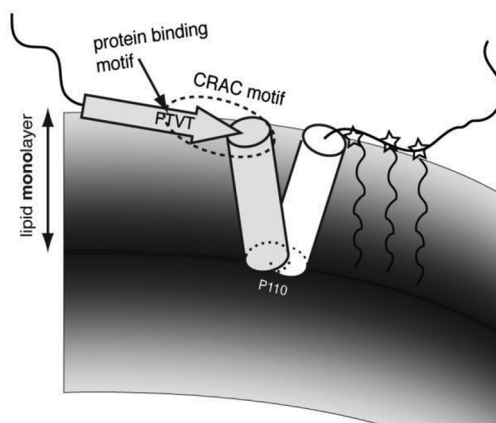

Figure 7. Schematic illustration of secondary structure distribution of membrane-bound Cav1. The wedge-shaped α-helical hairpin is too short to traverse the entire bilayer and occupies a single monolayer. The CSD is shown as largely β-stranded, with the putative CRAC motif present at the transition between β- and α-structure. The C-terminal palmitoylation sites are also indicated. Note that the exact orientation and structure of the β-strands remain uncertain and may well reflect an antiparallel β-hairpin instead of a single strand as shown, and that the protein is thought to be part of an oligomeric assembly (not shown).

Existing Structural Data and Models for the CSD.

Previous reports on Cav and the CSD fail to reach a consensus on the structure of the CSD. Studies by Fernandez et al. via CD and sequence analysis of a Cav$_{1-101}$ fragment in solution proposed the presence of an α-helix spanning residues 79−96.[19] Solution NMR and CD on solubilized Cav$_{82-101}$ also indicated a predominantly helical structure spanning residues

Ile84−Tyr97.[21] However, the latter experiments were largely done in the presence of the helicity-enhancing cosolvent TFE, which was reportedly required to avoid aggregation. CD spectroscopy on Cav$_{83−102}$ peptides associated with POPC vesicles[16] and Cav$_{82−101}$ peptides in DPC micelles[17] indicated only a partially α-helical structure for the isolated CSD. CD on a longer construct Cav$_{82−109}$ (also employed here) revealed a large increase in α-helicity, and solution NMR on the micelle-associated peptides localized the α-helical structure to residues 83−88 and 93−97 of the CSD and 102−108 within the IMD.[17] In some of these studies computational analysis of the primary sequence supported a predominantly α-helical CSD conformation, even leading to a predominantly helical full-length model of Cav.[4,19] On the other hand, an in silico study by Spisni et al. has proposed an antiparallel β-hairpin structure in residues 84−94 of the CSD, which is remarkably consistent with our findings.[24]

Despite the lack of consensus, our observations on membrane-bound peptides recapitulate a number of features reported above. We observe that the peptides are characterized by a partially α-helical conformation that is most pronounced in the C-terminal residues (beyond the CSD proper). The key difference in this study is the experimental identification of a β-stranded conformation within the CSD (in cholesterol-rich bilayers) and the fact that we site-specifically delineate the location of the different secondary structures. Our ssNMR results show that the observed mixed secondary structure content, with substantial nonhelical structure, is not simply due to sample heterogeneity (with some peptide largely helical but others unstructured) but rather reflects the presence of distinct domains within the peptides.

Our work is also distinct in that we probe the structure of the peptide in the presence of high levels of cholesterol to mimic the caveolar membrane and to facilitate examination of the CSD−cholesterol interaction. MAS and static ssNMR experiments clearly show that the lipid mixture responds to the integration of the peptides without generating peptide-induced heterogeneity in the lipids. Thus, we see a membrane-bound peptide and not simply the coprecipitation of noninteracting peptides and lipids.

Scaffolding Domain Functionalities. In the following sections, we will examine our observations in view of the different roles ascribed to the CSD, in an attempt to place our results in context and discuss potential implications for each of these CSD functionalities.

1. CSD Binding Partners. One critical caveolin function localized within the CSD relates to interactions with its numerous binding partners, such as protein G α-domains and Src family kinases.[13] Within the partner protein, this is mediated by the CBM, with a consensus sequence (ΦXΦXXXXΦXXΦ) rich in aromatic residues (Φ). The CBM of the protein G α-subunit forms a β-hairpin (Figure 8a)[13]. Within the CSD, residues F$_{92}$TVT$_{95}$ are involved, which adopt a β-stranded conformation in our samples. In various studies,[11,13,14,54,55] isolated short CSD peptides appear to emulate the effect of Cav binding to its binding partners, suggesting that the Cav tertiary structure is not required. Often a membrane is not present in those studies, raising the question of whether a membrane-bound CSD conformation is at all involved and thus how our data correlate to this CSD role.

2. Oligomerization. The CSD is also involved in the formation of Cav homo-oligomers, and oligomerization is a critical functionality as it appears to be required in the
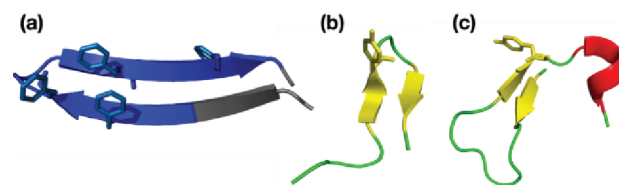

Figure 8. Secondary structure motifs in proposed homologous protein domains. (a) Structure of the aromatic-residue-rich caveolin binding sequence as originally identified in Gα proteins,[13] featuring a β-hairpin structure. (b, c) β-Strand-rich structures found among four putative CRAC motifs[59] in the PDC-109 crystal structure.[61] See Figure S5 for the complete protein context and additional details.

formation of caveolae. We note that a membrane-embedded β-stranded CSD may be prone to self-assemble into β-sheets in order to eliminate membrane-exposed non-hydrogen-bonded backbone sites. Indeed, a bioinformatics study by Spisni et al. has suggested that such a β-hairpin structure in residues 84−94 could play a role in homo-oligomer interactions.[24] It has also been noted that Cav1 appears to have a motif in residues 92−100, coinciding with the CSD, which strongly resembles the CBM.[13] This may indicate a mechanism for Cav self-oligomerization that is analogous to its recognition of the binding partner proteins. If so, this seems consistent with a potential CSD β-hairpin structure, given the hairpin conformation of the CBM (see above).

Our current data do not inform us on the oligomeric (or monomeric) nature of the peptides under investigation. Long-mixing $^{13}C−^{13}C$ experiments could be employed to identify intermolecular interactions and detect and characterize the supramolecular assemblies.[56,57] However, the long-mixing experiments on the current samples have failed to produce data consistent with intermolecular interactions, including experiments performed on samples prepared from mixtures of peptides p1 and p2 (not shown). This may be due to the sparse labeling and the relatively low signal intensities for some of the samples. More indirectly, the apparent rigidity of the peptides and pronounced effect on membrane fluidity could be indicative of the formation of peptide oligomers. However, this may also be explained in part by the high level of cholesterol present. Note that our data do show clear effects on the membrane dynamics and that the peptides are homogeneously associated with the membrane, resulting in a single population of lipid NMR as well as peptide signals. This indicates that any oligomerization that has occurred is taking place in a membrane-bound state and thus may be mimicking the homo-oligomer formation that Cav displays in cholesterol-rich caveolae.

3. Cholesterol Binding. The binding of cholesterol is thought to be mediated by residues V$_{94}$TKYWFYR$_{101}$ that form a putative CRAC motif. The original CRAC motif was identified in the translocator protein TSPO.[58] Subsequent solution NMR studies of various CRAC motifs have proposed a predominantly α-helical CRAC structure,[17,20,22] although other work suggested a lower level of α-helicity.[16] This difference has been credited to a loss of helical structure due to truncation in the shorter peptides used in the latter studies.[17] The above structural work involved short peptides lacking protein context, but a recent study reported on CRAC motifs in the protein PDC-109, for which a known homologous structure exists.[59] While this seemingly provides much-needed high-resolution structures of these motifs in a native context, a more detailed

inspection reveals an array of different structures (Figure 8b,c and Figure S5). This may act as a reminder that these are *putative* motifs and that some may not be functional cholesterol binding domains. Nonetheless, while PDC-109 fails to provide an unambiguous structure for the CRAC motif, it may provide examples of possible β-rich CRAC conformations (Figure 8b,c). Both our experimental and computational data indicate a specific transition of β-sheet to α-helical structure to occur within the CRAC motif, near the motif's conserved central Tyr97, reminiscent of earlier computational predictions.[24] Intriguingly, at least one of the PDC-109 CRAC motifs (Figure 8c) shows a similar motif, with the central Tyr at the C-terminal end of a β-hairpin and near the start of a flanking helical segment. The observed sheet−helix transition is also reminiscent of the tendency for CRAC motifs to occur directly adjacent to transmembrane helices.[60]

Given the reported strong interactions between caveolin and cholesterol, one key point of interest will be to characterize this interaction in more detail in future work. Interestingly, in the current work we have not seen large effects for the peptide NMR signals of the omission of cholesterol (Figure S1). This suggests that the observed secondary structures are not directly correlated to cholesterol binding, raising the question of whether this indicates a more subtle effect of cholesterol binding, the need for other parts of Cav, or a role for other lipids enriched in caveolae (e.g., sphingomyelin).

The above shows that there have been indications of a role for β-stranded conformations in CSD and that such a structure may make sense from a functional point of view. One seemingly common feature is the presence of β-hairpins, as also suggested by Spisni et al., who proposed that an antiparallel β-hairpin is formed by residues 84−94.[24] Our ssNMR data reveal the localized β-conformation, but having thus far failed to observe long-distance inter- or intramolecular interactions, it remains uncertain whether this represents a single β-strand or shorter β-strands within e.g. a β-hairpin. The relatively sparse labeling applied here makes it impossible to exclude the hairpin motif based on these data, as it is quite possible that labeled sites in a β-hairpin would be too far apart. Whether in a hairpin or not, it may well be that the β-strands play a role in the oligomerization process, as membrane-embedded strands could be driven to self-assemble to prevent exposure of the peptide backbones to the hydrophobic membrane environment.[24]

■ CONCLUSION

Our experimental and computational analysis of the structural features of Cav1 fragments seems to indicate a more significant propensity for β-sheet structures with the CSD than apparent from the existing literature. We have discussed that such β-rich structures could be consistent with its various functionalities, while highlighting the need for further characterization. One important consideration is that the caveolins fulfill a variety of functions, which could be independent of each other, occur in different locations within the cell, and may involve different Cav conformations. For instance, it has been pointed out that palmitoylation is nonessential for the localization in caveolae but that it is critical for the cholesterol trafficking by Cav.[10] It seems likely that the Cav conformation within caveolae could be significantly different from its structure in a cholesterol-bound cytosolic state. Thus, it is important to investigate Cav structure in different contexts, including cholesterol-rich membranes as examined here. Thus, far, we lack a clear understanding of the structural effects of cholesterol binding, as

we did not observe a large structural change in the presence of cholesterol. Clearly, additional experimental and structural data will be critical to elucidate the conformation and oligomeric states of Cav and to provide an understanding of the effect of disease-causing mutations and the structural underpinning of its many functional roles within the cell.

■ ASSOCIATED CONTENT

Ⓢ Supporting Information

Table of labeled peptides; detailed experimental conditions for ssNMR experiments; peptide concentration and cholesterol dependence of ^{13}C and ^{31}P NMR spectra; secondary structure content estimates from FTIR; ^{13}C chemical shift assignments; additional FTIR and CD spectra; additional 2D ^{13}C−^{13}C spectra and secondary structure predictions; structures of related proteins. This material is available free of charge via the Internet at http://pubs.acs.org.

■ AUTHOR INFORMATION

Corresponding Author
*Phone: +1-412-383-9896. E-mail: pvdwel@pitt.edu.

Present Address
‡Department of Chemistry & Biochemistry, 251 Nieuwland Science Hall, University of Notre Dame du Lac, Notre Dame, IN 46556.

Author Contributions
†These authors contributed equally to this work.

■ ACKNOWLEDGMENTS

■ ABBREVIATIONS

Cav, caveolin; CBM, caveolin-binding motif; CP, cross-polarization; CRAC, cholesterol recognition/interaction amino acid consensus; CSA, chemical shift anisotropy; CSD, caveolin scaffolding domain; CSI, chemical shift indexing; DARR, dipolar-assisted rotational resonance; DPC, dodecyl-phosphocholine; IMD, intramembrane domain; MAS, magic angle spinning; PDSD, proton-driven spin diffusion; POPC, 1-palmitoyl-2-oleoyl-*sn*-glycero-3-phosphocholine; ssNMR, solid-state NMR; TFE, trifluoroethanol; TPPM, two-pulse phase modulation.

■ REFERENCES

(1) Razani, B., Woodman, S. E., and Lisanti, M. P. (2002) Caveolae: from cell biology to animal physiology. *Pharmacol. Rev. 54*, 431−467.

(2) Anderson, R. G. W. (1998) The caveolae membrane system. *Annu. Rev. Biochem. 67*, 199−225.

(3) Parton, R. G., and Simons, K. (2007) The multiple faces of caveolae. *Nat. Rev. Mol. Cell Biol. 8*, 185−194.

(4) Parton, R. G., Hanzal-Bayer, M., and Hancock, J. F. (2006) Biogenesis of caveolae: a structural model for caveolin-induced domain formation. *J. Cell Sci. 119*, 787−796.

(5) Engelman, J. A., Zhang, X., Galbiati, F., Volonte, D., Sotgia, F., Pestell, R. G., Minetti, C., Scherer, P. E., Okamoto, T., and Lisanti, M. P. (1998) Molecular genetics of the caveolin gene family: implications for human cancers, diabetes, Alzheimer disease, and muscular dystrophy. *Am. J. Hum. Genet. 63*, 1578−1587.

(6) Ostermeyer, A. G., Ramcharan, L. T., Zeng, Y., Lublin, D. M., and Brown, D. A. (2004) Role of the hydrophobic domain in targeting caveolin-1 to lipid droplets. *J. Cell Biol. 164*, 69–78.

(7) Aoki, S., Thomas, A., Decaffmeyer, M., Brasseur, R., and Epand, R. M. (2010) The role of proline in the membrane re-entrant helix of caveolin-1. *J. Biol. Chem. 285*, 33371–33380.

(8) Li, S., Song, K. S., and Lisanti, M. P. (1996) Expression and characterization of recombinant caveolin. Purification by polyhistidine tagging and cholesterol-dependent incorporation into defined lipid membranes. *J. Biol. Chem. 271*, 568–573.

(9) Dietzen, D. J., Hastings, W. R., and Lublin, D. M. (1995) Caveolin is palmitoylated on multiple cysteine residues. Palmitoylation is not necessary for localization of caveolin to caveolae. *J. Biol. Chem. 270*, 6838–6842.

(10) Uittenbogaard, A., and Smart, E. J. (2000) Palmitoylation of caveolin-1 is required for cholesterol binding, chaperone complex formation, and rapid transport of cholesterol to caveolae. *J. Biol. Chem. 275*, 25595–25599.

(11) Li, S., Couet, J., and Lisanti, M. P. (1996) Src tyrosine kinases, Galpha subunits, and H-Ras share a common membrane-anchored scaffolding protein, caveolin. Caveolin binding negatively regulates the auto-activation of Src tyrosine kinases. *J. Biol. Chem. 271*, 29182–29190.

(12) Schlegel, A., Schwab, R. B., Scherer, P. E., and Lisanti, M. P. (1999) A role for the caveolin scaffolding domain in mediating the membrane attachment of caveolin-1. The caveolin scaffolding domain is both necessary and sufficient for membrane binding in vitro. *J. Biol. Chem. 274*, 22660–22667.

(13) Couet, J., Li, S., Okamoto, T., Ikezu, T., and Lisanti, M. P. (1997) Identification of peptide and protein ligands for the caveolin-scaffolding domain. Implications for the interaction of caveolin with caveolae-associated proteins. *J. Biol. Chem. 272*, 6525–6533.

(14) Couet, J., Sargiacomo, M., and Lisanti, M. P. (1997) Interaction of a receptor tyrosine kinase, EGF-R, with caveolins. Caveolin binding negatively regulates tyrosine and serine/threonine kinase activities. *J. Biol. Chem. 272*, 30429–30438.

(15) Murata, M., Peränen, J., Schreiner, R., Wieland, F., Kurzchalia, T. V., and Simons, K. (1995) VIP21/caveolin is a cholesterol-binding protein. *Proc. Natl. Acad. Sci. U. S. A. 92*, 10339–10343.

(16) Epand, R. M., Sayer, B. G., and Epand, R. F. (2005) Caveolin scaffolding region and cholesterol-rich domains in membranes. *J. Mol. Biol. 345*, 339–350.

(17) Le Lan, C., Neumann, J. M., and Jamin, N. (2006) Role of the membrane interface on the conformation of the caveolin scaffolding domain: a CD and NMR study. *FEBS Lett. 580*, 5301–5305.

(18) Levin, A. M., Coroneus, J. G., Cocco, M. J., and Weiss, G. A. (2006) Exploring the interaction between the protein kinase A catalytic subunit and caveolin-1 scaffolding domain with shotgun scanning, oligomer complementation, NMR, and docking. *Protein Sci. 15*, 478–486.

(19) Fernandez, I., Ying, Y., Albanesi, J., and Anderson, R. G. W. (2002) Mechanism of caveolin filament assembly. *Proc. Natl. Acad. Sci. U. S. A. 99*, 11193–11198.

(20) Le Lan, C., Gallay, J., Vincent, M., Neumann, J. M., de Foresta, B., and Jamin, N. (2010) Structural and dynamic properties of juxta-membrane segments of caveolin-1 and caveolin-2 at the membrane interface. *Eur. Biophys. J. 39*, 307–325.

(21) Levin, A. M., Murase, K., Jackson, P. J., Flinspach, M. L., Poulos, T. L., and Weiss, G. A. (2007) Double barrel shotgun scanning of the caveolin-1 scaffolding domain. *ACS Chem. Biol. 2*, 493–500.

(22) Jamin, N., Neumann, J. M., Ostuni, M. A., Vu, T. K. N., Yao, Z.-X., Murail, S., Robert, J.-C., Giatzakis, C., Papadopoulos, V., and Lacapère, J.-J. (2005) Characterization of the cholesterol recognition amino acid consensus sequence of the peripheral-type benzodiazepine receptor. *Mol. Endocrinol. 19*, 588–594.

(23) Ortegren, U., Karlsson, M., Blazic, N., Blomqvist, M., Nystrom, F. H., Gustavsson, J., Fredman, P., and Strålfors, P. (2004) Lipids and glycosphingolipids in caveolae and surrounding plasma membrane of primary rat adipocytes. *Eur. J. Biochem. 271*, 2028–2036.

(24) Spisni, E., Tomasi, V., Cestaro, A., and Tosatto, S. C. E. (2005) Structural insights into the function of human caveolin 1. *Biochem. Biophys. Res. Commun. 338*, 1383–1390.

(25) McDermott, A. (2009) Structure and dynamics of membrane proteins by magic angle spinning solid-state NMR. *Annu. Rev. Biophys. 38*, 385–403.

(26) Hong, M. (2006) Oligomeric structure, dynamics, and orientation of membrane proteins from solid-state NMR. *Structure 14*, 1731–1740.

(27) Opella, S. J., and Marassi, F. M. (2004) Structure determination of membrane proteins by NMR spectroscopy. *Chem. Rev. 104*, 3587–3606.

(28) Smith, S. O., Eilers, M., Song, D., Crocker, E., Ying, W., Groesbeek, M., Metz, G., Ziliox, M., and Aimoto, S. (2002) Implications of threonine hydrogen bonding in the glycophorin A transmembrane helix dimer. *Biophys. J. 82*, 2476–2486.

(29) Bennett, A. E., Rienstra, C. M., Auger, M., Lakshmi, K. V., and Griffin, R. G. (1995) Heteronuclear decoupling in rotating solids. *J. Chem. Phys. 103*, 6951–6958.

(30) Luo, W., and Hong, M. (2010) Conformational changes of an ion channel detected through water-protein interactions using solid-state NMR spectroscopy. *J. Am. Chem. Soc. 132*, 2378–2384.

(31) Takegoshi, K., Nakamura, S., and Terao, T. (2001) C-13-H-1 dipolar-assisted rotational resonance in magic-angle spinning NMR. *Chem. Phys. Lett. 344*, 631–637.

(32) Forbes, J., Bowers, J., Shan, X., Moran, L., Oldfield, E., and Moscarello, M. A. (1988) Some new developments in solid-state nuclear magnetic resonance spectroscopic studies of lipids and biological membranes, including the effects of cholesterol in model and natural systems. *J. Chem. Soc., Faraday Trans. 1 84*, 3821–3849.

(33) Guo, W., and Hamilton, J. A. (1996) 13C MAS NMR studies of crystalline cholesterol and lipid mixtures modeling atherosclerotic plaques. *Biophys. J. 71*, 2857–2868.

(34) Delaglio, F., Grzesiek, S., Vuister, G. W., Zhu, G., Pfeifer, J., and Bax, A. (1995) NMRPipe: a multidimensional spectral processing system based on UNIX pipes. *J. Biomol. NMR 6*, 277–293.

(35) Goddard, T. D., and Kneller, D. G. *Sparky*, 3rd ed.; University of California: San Francisco.

(36) Vranken, W. F., Boucher, W., Stevens, T. J., Fogh, R. H., Pajon, A., Llinas, M., Ulrich, E. L., Markley, J. L., Ionides, J., and Laue, E. D. (2005) The CCPN data model for NMR spectroscopy: development of a software pipeline. *Proteins 59*, 687–696.

(37) Harris, R. K., Becker, E. D., De Menezes, S. M. C., Granger, P., Hoffman, R. E., and Zilm, K. W. (2008) Further conventions for NMR shielding and chemical shifts (IUPAC Recommendations 2008). *Magn. Reson. Chem. 46*, 582–598.

(38) Jones, D. T. (1999) Protein secondary structure prediction based on position-specific scoring matrices. *J. Mol. Biol. 292*, 195–202.

(39) Rost, B., Yachdav, G., and Liu, J. (2004) The PredictProtein server. *Nucleic Acids Res. 32*, W321–326.

(40) Montgomerie, S., Cruz, J. A., Shrivastava, S., Arndt, D., Berjanskii, M., and Wishart, D. S. (2008) PROTEUS2: a web server for comprehensive protein structure prediction and structure-based annotation. *Nucleic Acids Res. 36*, W202–209.

(41) Dufourc, E. J., Mayer, C., Stohrer, J., Althoff, G., and Kothe, G. (1992) Dynamics of phosphate head groups in biomembranes. Comprehensive analysis using phosphorus-31 nuclear magnetic resonance lineshape and relaxation time measurements. *Biophys. J. 61*, 42–57.

(42) Van der Wel, P. C. A., Pott, T., Morein, S., Greathouse, D. V., Koeppe, R., and Killian, J. (2000) Tryptophan-anchored transmembrane peptides promote formation of nonlamellar phases in phosphatidylethanolamine model membranes in a mismatch-dependent manner. *Biochemistry 39*, 3124–3133.

(43) Costello, A. L., and Alam, T. M. (2010) Investigating the impact of cholesterol on magnetically aligned sphingomyelin/cholesterol multilamellar vesicles using static (31)P NMR. *Chem. Phys. Lipids 163*, 506–513.

(44) Holland, G. P., McIntyre, S. K., and Alam, T. M. (2006) Distinguishing individual lipid headgroup mobility and phase transitions in raft-forming lipid mixtures with 31P MAS NMR. *Biophys. J. 90*, 4248−4260.

(45) Huang, J., and Feigenson, G. W. (1999) A microscopic interaction model of maximum solubility of cholesterol in lipid bilayers. *Biophys. J. 76*, 2142−2157.

(46) Benetis, N., Kyrikou, I., Zervou, M., and Mavromoustakos, T. (2005) Static CP P-31 NMR multilamellar bilayer broadlines in the absence and presence of the bioactive dipeptide beta-Ala-Tyr or Glu. *Chem. Phys. 314*, 57−72.

(47) Seelig, J. (1978) P-31 nuclear magnetic-resonance and head group structure of phospholipids in membranes. *Biochim. Biophys. Acta 515*, 105−140.

(48) Kong, J., and Yu, S. (2007) Fourier transform infrared spectroscopic analysis of protein secondary structures. *Acta Biochim. Biophys. Sin. 39*, 549−559.

(49) Reis, O., Winter, R., and Zerda, T. W. (1996) The effect of high external pressure on DPPC-cholesterol multilamellar vesicles: a pressure-tuning Fourier transform infrared spectroscopy study. *Biochim. Biophys. Acta 1279*, 5−16.

(50) Wishart, D. S., and Sykes, B. D. (1994) The 13C Chemical-Shift Index: A simple method for the identification of protein secondary structure using 13C chemical-shift data. *J. Biomol. NMR 4*, 171−180.

(51) Zhang, H., Neal, S., and Wishart, D. S. (2003) RefDB: a database of uniformly referenced protein chemical shifts. *J. Biomol. NMR 25*, 173−195.

(52) Senes, A., Engel, D. E., and DeGrado, W. F. (2004) Folding of helical membrane proteins: the role of polar, GxxxG-like and proline motifs. *Curr. Opin. Struct. Biol. 14*, 465−479.

(53) Morris, R., Cox, H., Mombelli, E., and Quinn, P. J. (2004) Rafts, little caves and large potholes: how lipid structure interacts with membrane proteins to create functionally diverse membrane environments. *Subcell. Biochem. 37*, 35−118.

(54) Volonte, D., and Galbiati, F. (2009) Inhibition of thioredoxin reductase 1 by caveolin 1 promotes stress-induced premature senescence. *EMBO Rep. 10*, 1334−1340.

(55) Toya, Y., Schwencke, C., Couet, J., Lisanti, M. P., and Ishikawa, Y. (1998) Inhibition of adenylyl cyclase by caveolin peptides. *Endocrinology 139*, 2025−2031.

(56) Lewandowski, J. R., van der Wel, P. C. A., Rigney, M., Grigorieff, N., and Griffin, R. G. (2011) Structural Complexity of a Composite Amyloid Fibril. *J. Am. Chem. Soc. 133*, 14686−14698.

(57) Li, J., Hoop, C. L., Kodali, R., Sivanandam, V. N., and van der Wel, P. C. A. (2011) Amyloid-like fibrils from a domain-swapping protein feature a parallel, in-register conformation without native-like interactions. *J. Biol. Chem. 286*, 28988−28995.

(58) Li, H., and Papadopoulos, V. (1998) Peripheral-type benzodiazepine receptor function in cholesterol transport. Identification of a putative cholesterol recognition/interaction amino acid sequence and consensus pattern. *Endocrinology 139*, 4991−4997.

(59) Scolari, S., Müller, K., Bittman, R., Herrmann, A., and Müller, P. (2010) Interaction of mammalian seminal plasma protein PDC-109 with cholesterol - Implications for a putative CRAC domain. *Biochemistry 49*, 9027−9031.

(60) Epand, R. M. (2008) Proteins and cholesterol-rich domains. *Biochim. Biophys. Acta 1778*, 1576−1582.

(61) Wah, D. A., Fernández-Tornero, C., Sanz, L., Romero, A., and Calvete, J. J. (2002) Sperm coating mechanism from the 1.8 A crystal structure of PDC-109-phosphorylcholine complex. *Structure 10*, 505−514.